# Visible organized structures in large pool fires
## *types and time dependent properties*

*Axel Schönbucher*
Christoph Balluff,
Dietmar Göck,
Christian Kuhr,
Iris Vela,

Presentation at ICES
University of Utah
May 10th – 12th, 2006

University of Duisburg-Essen
Institute of Chemical Engineering
Germany



# Visible organized structures in large pool fires
## *types and time dependent properties*

*Axel Schönbucher*
Christoph Balluff,
Dietmar Göck,
Christian Kuhr,
Iris Vela

Workshop on Fire Models & Validation
Workshop on Heat Transfer in Fires
Albuquerque NM, USA
May 07th – 09th, 2006

University of Duisburg-Essen
Institute of Chemical Engineering
Germany

A. Schönbucher Institute of Chemical Engineering
UNIVERSITÄT DUISBURG ESSEN

# Visible organized structures in large pool fires
## *types and time dependent properties*

1. Introduction
2. Experimental
3. Types of visible organized structures
4. Instantaneous properties





# 1. Introduction

- In this presentation a short survey is given on our work on the observed instantaneous behaviour of large pool fires.
- At present only few instantaneous properties of the observed organized structures in pool fires can be predicted with the CFD simulation methods.

# 2. Experimental

Large-scale pool fire experiments:

$1\ m \leq d \leq 25\ m$

n-pentane, premium gasoline, regular grade gasoline, diesel, JP-4

Visualization methods to record organized structures:

- Schlieren records ($d \leq 0.5$ m)
- Holographic real time interferometry ($d \leq 0.3$ m)
- Direct photographic records ($0.4\ \mu m < \lambda < 0.75\ \mu m$)
- Thermographic camera system ($2\ \mu m < \lambda < 5.6\ \mu m$)
- Pyroelectric radiometer system ($0.6\ \mu m < \lambda < 15\ \mu m$)
- Meteorological station





# 3. Types of visible organized structures

The observed organized structures can be classified into the following two main types:

(I) *Luminous* (from light-yellow to dark orange) structures:

- Luminous band (luminous flame zone)
- Contour flame parcels
- Axial flame parcels
- Hot spots
- Rotating flame columns (fire whirls)

(II) *Dark* (from grey to black) structures

- Contour soot parcels
- Axial soot parcels
- Soot plume or rather clouds of smoke

It is often observed that luminous structures change to dark structures.

# 3. Types of visible organized structures

## 3.1 Qualitative description

Structures with the following different natures occur:

- *Statistical* or rather instationary,
- Localized or rather stationary,
- Periodical,
- Quasi-periodical

*Occurrence* and *specific properties* of the organized structures depend on the:

- Pool diameter d,
- Type of the fuel which is burning,
- Wind field (value and direction of the wind) which surrounds the flame.





# 3. Types of visible organized structures

## 3.1.1 Luminous band

**Luminous band; n-pentane pool fire (d = 25 m)**

**The luminous band has the following properties:**

- **Ring shaped light luminous zone with a diameter $d_{LB}$ and a height $h_{LB}$ directly above the liquid fuel surface**
- **$h_{LB} \approx 0.1$ d to 0.3 d**
- **$d_{LB}(x)$ decreases with increasing height x above the pool rim**
- **At the upper edge of the luminous band the formation of dark soot particles occurs for the first time**

## 3.1.2 Contour flame parcels and contour soot parcels

Contour *flame* parcels (left) and contour *soot* parcels (right); n-pentane pool fire (d = 25 m)

- At heights $1 < x/d < 1.5$ and for n-pentane flames up to $x/d \approx 2.5$, contour parcels are formed. These contour parcels are responsible for the shape and radiation properties of pool fires. The contour parcels are hemispherical to spherical volumina which rise at the contour of the flame by expansion.
- During the buoyancy driven rise a *rotation* of the contour parcels can be observed.





## 3.1.3 Axial flame parcels and axial soot parcels

kerosene pool fire (d = 25 m)

- Unlike the contour parcels the axial parcels are symmetrical to the flame axis, much larger and the formation occurs periodically. It is characteristic that the axial parcels show a *rotation*.
- Mostly the surface of the bulge is horizontally ring-shaped and is covered from the beginning with dark soot.
- The rising bulge enlarges his diameter whereas the inside of the flame contracts. In this way an axial parcel is formed.

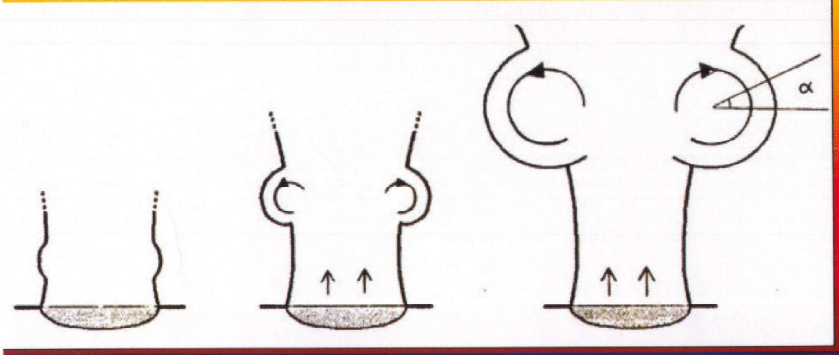


Formation and rising of the axial parcel in a pool fire; α: revolution angle

## 3.1.3 Axial flame parcels and axial soot parcels

- For x/d > 0.8 the buoyant acceleration $\bar{b}$ becomes smaller at the contour surfaces until $\bar{b} \rightarrow 0$. In the range near the flame axis $\bar{b}$ is still larger than at the contour; so a *mushroom shaped* structure is formed:

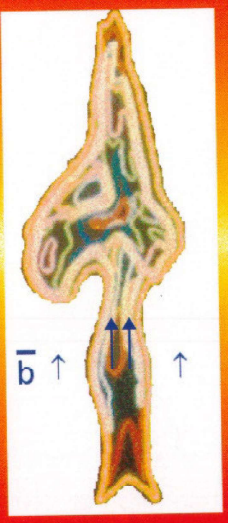


n-hexane (d = 4.6 cm)





## 3.1.4 Hot spots

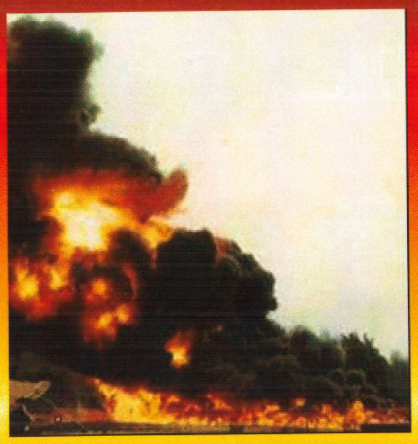

Hot spot (hs) in a JP-4 pool fire (d = 25 m)

- The hot spots are *luminous* in the spectral range between light yellow to dark orange. Radiation of the hot spots is very intensive.
- The shapes are very irregular. The hot spots are formed statistically and appear at the outer surface of the fire. Often they appear near a contour parcel or near an axial parcel the volume of which is increased strongly.
- The hot spots are formed inside the flame near the flame axis and a motion in radial direction occurs.

## 3.1.5 Soot plume

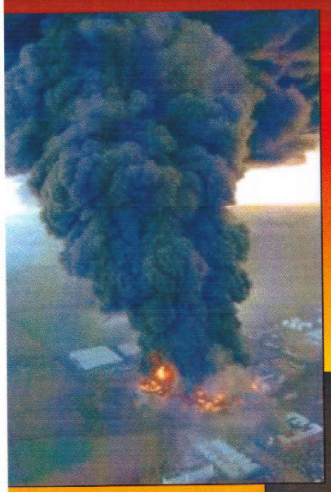

- In a soot plume, contour flame parcels, axial flame parcels and hot spots no longer exist.
- The temperature $T_{sp}$ of the soot particles is relatively low.
- The plume is composed of soot clouds. They show a strong or weak dispersion, depending on the stability of the atmosphere.

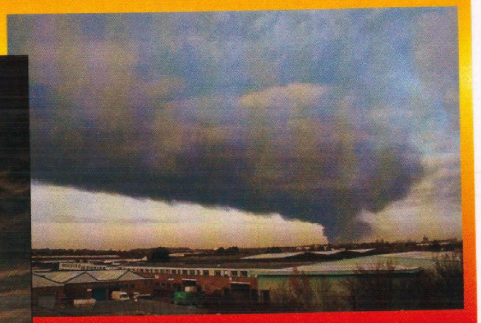

Buncefield
12/11/05





## 3.1.6 Rotating flame columns

- The rotating column (rc) has a height to diameter ratio between $3 < h_{rc}/d_{rc} < 5$. Due to the buoyancy the rotating columns have a vertical translational motion. This means a *screw-shaped* motion of the rotating columns.

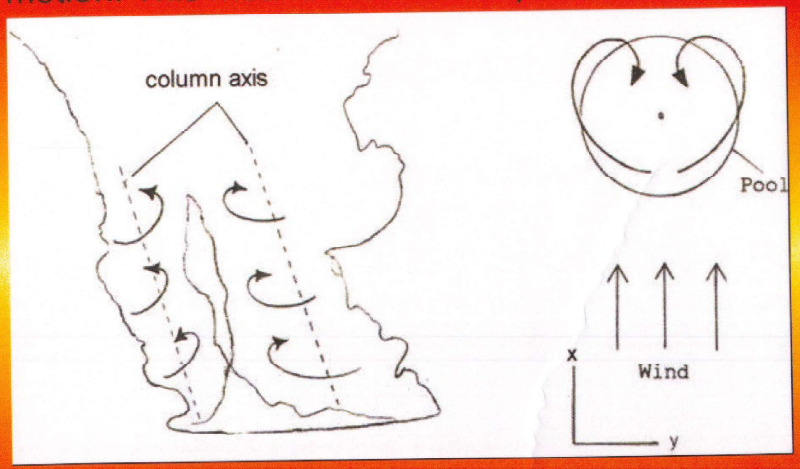


- Leeward two contra-rotating columns are observed. For the n-pentane and premium gasoline pool fires (d = 25 m) the heights hrc and diameters $d_{rc}$ of the columns are in the ranges: $0.75 < h_{rc}/d < 0.8$ and $0.12 < d_{rc}/d < 0.2$.

## 3.1.6 Rotating flame columns

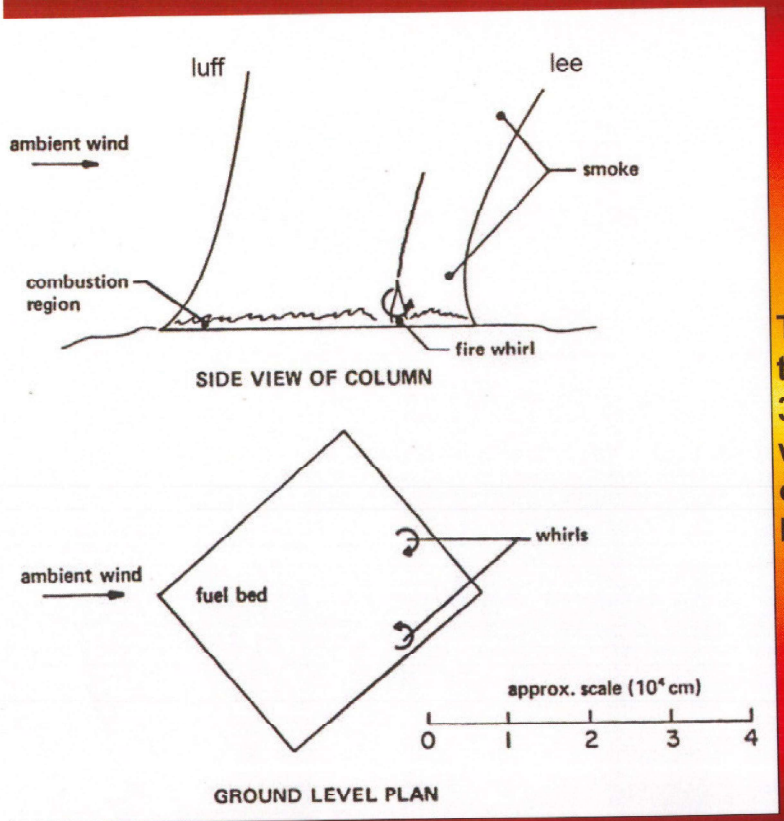


The formation of fire whirls at the edge of a large scale 300 m x 400 m wooden fire under the influence of wind; by *Corlett*.





## 3.2 Quantities which influence the organized structures

The observed types of organized structures are influenced by the following chemical and physical quantities, the:

- fuel which burns as a pool fire
- pool diameter d
- wind velocity and wind direction.

*Balluff* has investigated in his thesis the influence of fuel, pool diameter d and the wind velocity (and direction) on the 6 types of organized structures.

# 4. Instantaneous properties
## 4.1 Geometric characteristics
### 4.1.1 Flame height H, flame tilt Θ

The flame height H, the flame diameter $d_F$ and the flame tilt Θ fluctuate and depend on time t, pool diameter d, burning rate $v_a$ and wind velocity $u_w$.

For the prediction of the mean there exist several semi-empirical equations (e.g. *Thomas*, *Moorhouse*).

With OSRAMO II a new equation for $\overline{v}_a$ (d, $M_{fp,tot}$(d), $r_p$) exists.





### 4.1.2 Flame contours

- for d ≥ 25 m the flame column losses its coherence and a splitting (separation) into several rotating flame columns occurs.
- In a large pool fire a splitting into rotating flame columns occurs if the following criteria for the dimensionless heat flow rate [-] is valid:

$$\dot{Q}^* \leq \frac{\rho_f v_a (-\Delta h_c)}{c_{p,F}\, \rho_0\, T_0 \sqrt{g}} \frac{1}{\sqrt{d}}$$

The measured *small scale* contours of pool fires at various diameters d.

At present it is *not* possible to predict the small scale contours of pool fires.

## 4.1.2 Flame contours

In large pool fires the instantaneous contours are dominated by the dynamic behaviour of the parcels (e.g. axial parcels, soot parcels, hot spots, contour parcels). An approximately prediction (Nakakuki (1974)) of the flame contours is only possible for very small fires (d  3.5 cm). For visualizing instantaneous contours the authors have used the following methods:

- Schlieren records (d ≤ 50 cm)
- Holographic real-time interferometry (d ≤ 30 cm)
- Direct photographic records in the VIS-spectral range (any d)
- Thermographic images in the IR-spectral range (any d).

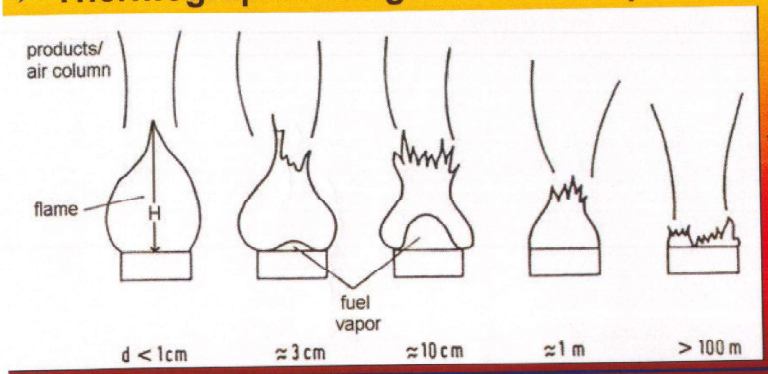


Instantaneous flame contours which depend on the pool diameter d, without considering the small scale shape; by *Corlett*





## 4.1.3 Flame diameter $d_F$

- In contrast to all flame tilt correlations the flame diameter $d_F(t)$ remains not constant with increasing x/d at higher wind velocities $u_w$ with a flame tilt angle Θ > 20°

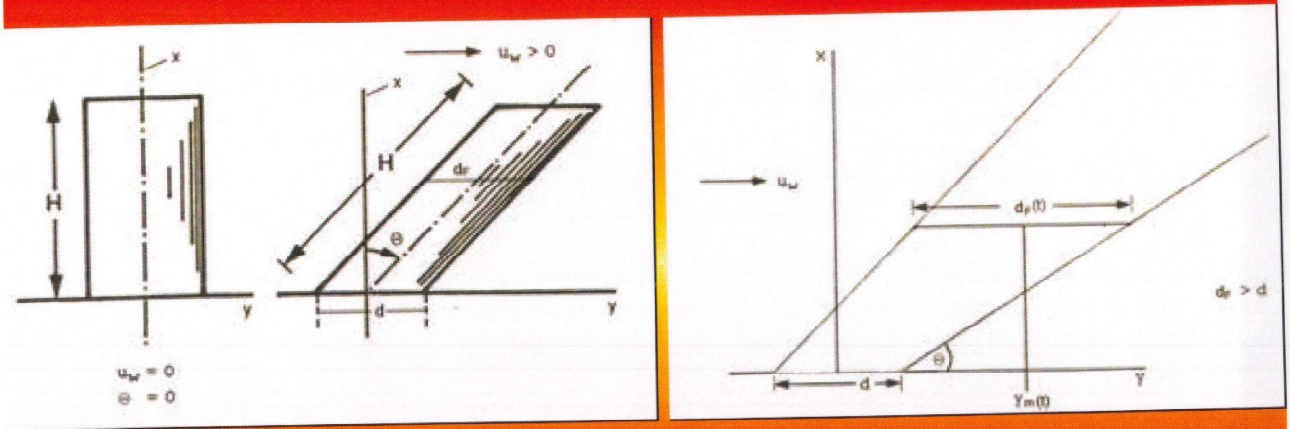


Flame diameter $d_F$ at small Θ (left) and $d_F(t,x)$ larger Θ > 20° (right) in pool fires; $y_m(t)$: coordinate of the centre of the flame.

## 4.1.3 Flame diameter $d_F$

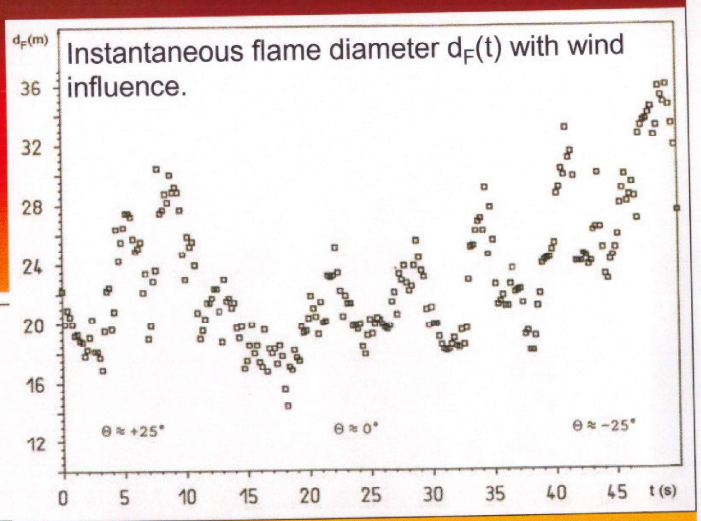


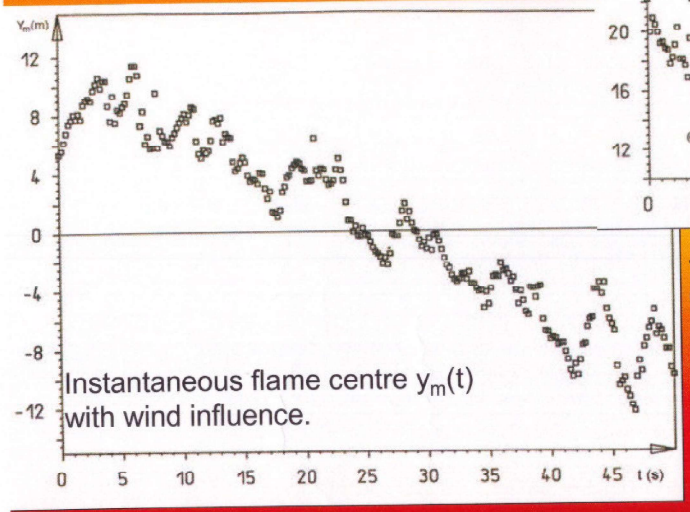


JP-4/gasoline pool fire
(d = 25 m, x/d = 0.9)





## 4.1.3 Flame diameter $d_F$

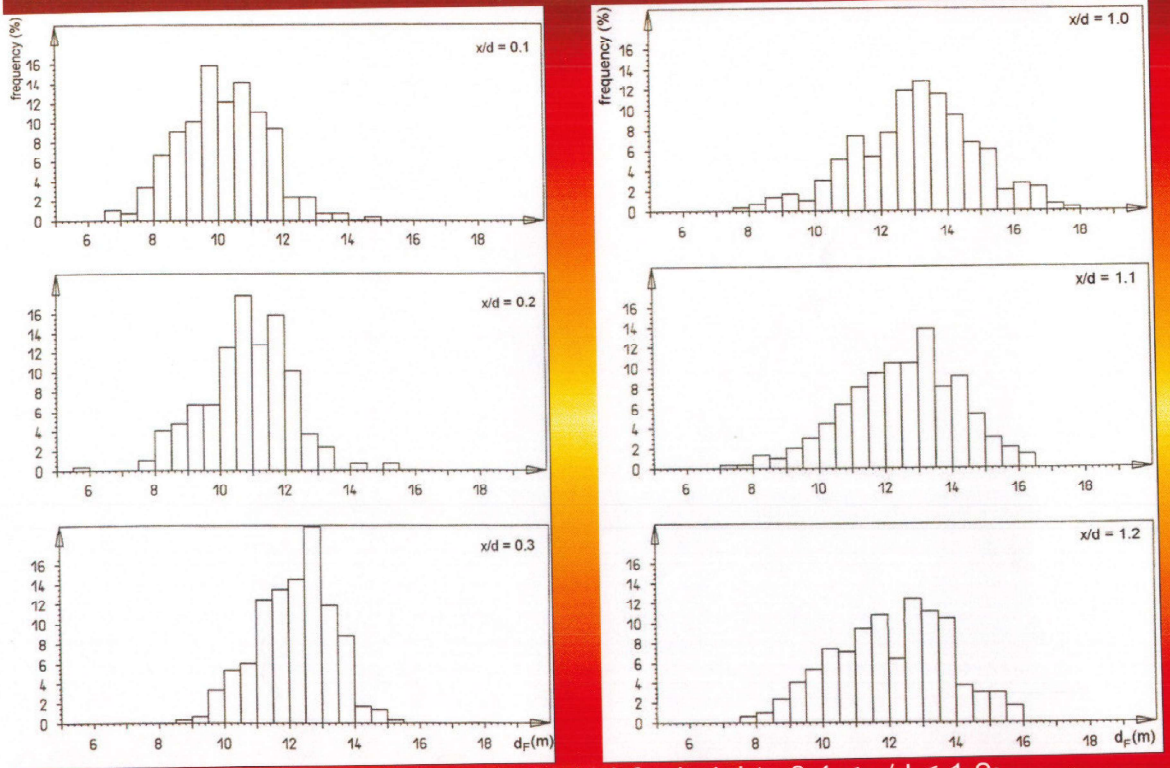


Frequency distributions [histograms] $h(d_F)$ for heights $0.1 \le x/d \le 1.2$:
n-pentane pool fire (d = 25 m)

## 4.2 Translation velocities of axial parcels

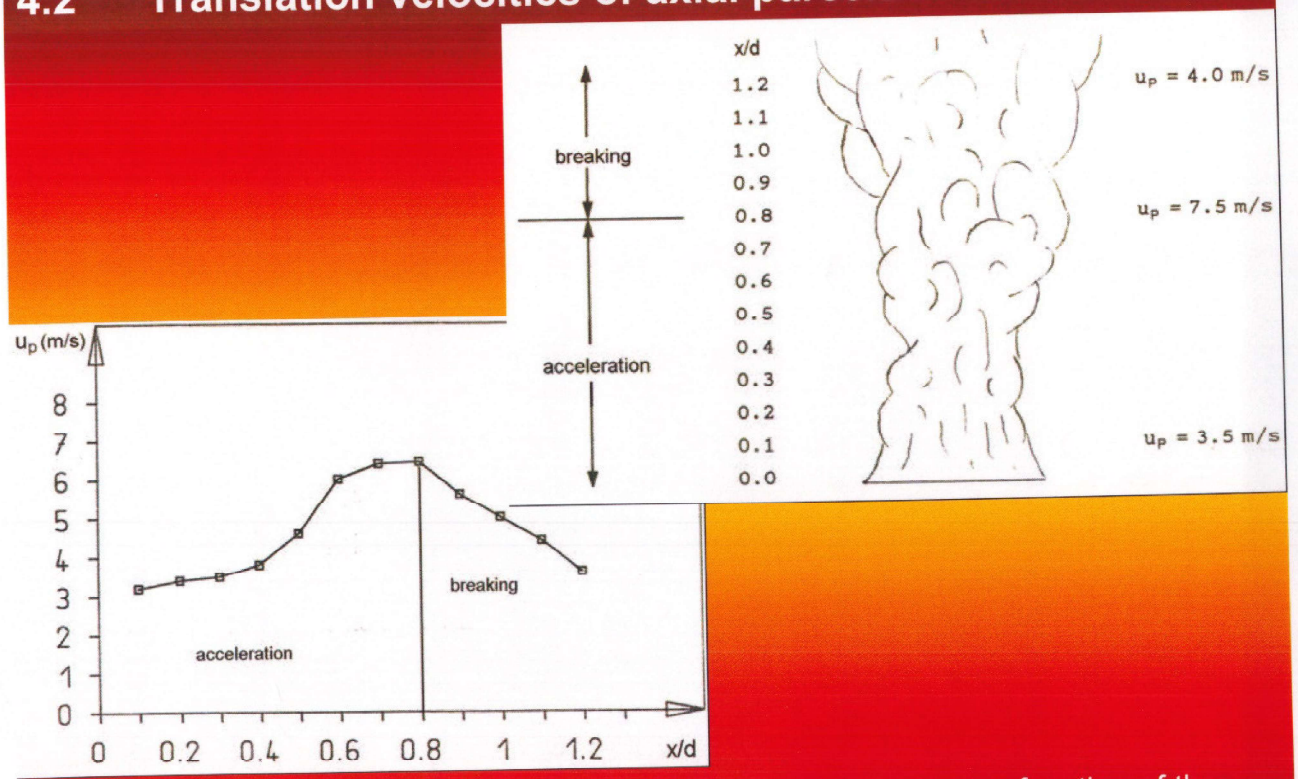


Instantaneous translation velocities $u_p(x/d)$ of rising axial parcels as a function of the relative height x/d; JP-4/gasoline pool fire (d = 16 m)





## 4.2 Translation velocities of axial parcels

$u_p(x)$: *instantaneous* (translation) velocity in x-direction, averaged over the number of parcels.

$\bar{u}_p$ (translation) velocity, averaged over the rising time, the number of parcels and the height x.

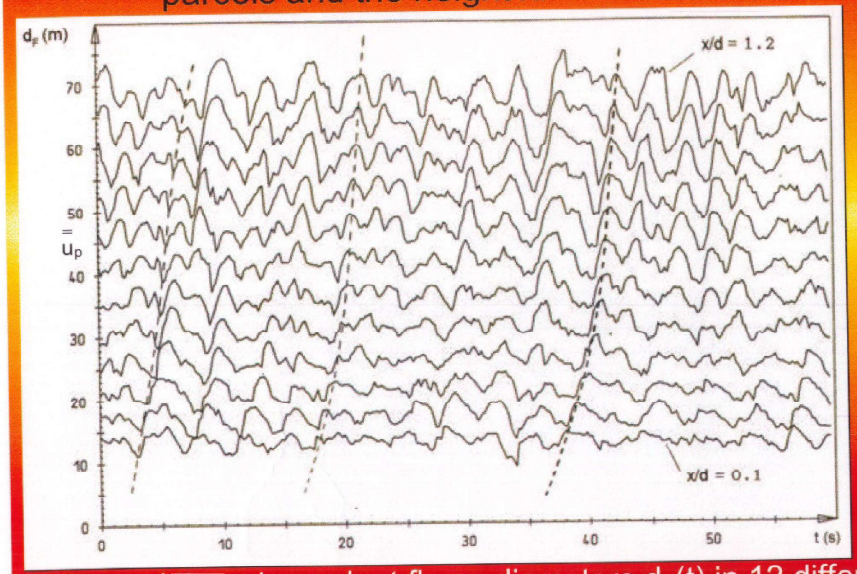


Measured time-dependent flame diameters $d_F(t)$ in 12 different heights x/d with offset; JP-4/gasoline pool fire (d = 16 m)

## 4.2 Translation velocities of axial parcels

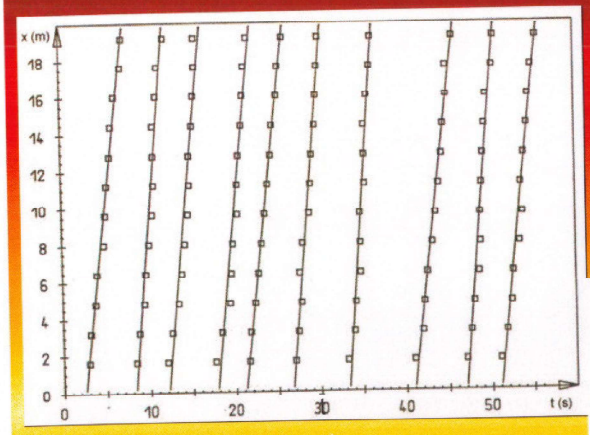


Heights x reached by the extreme values of $d_F(t)$ as a function of time t; JP-4/gasoline pool fire (d = 16 m)

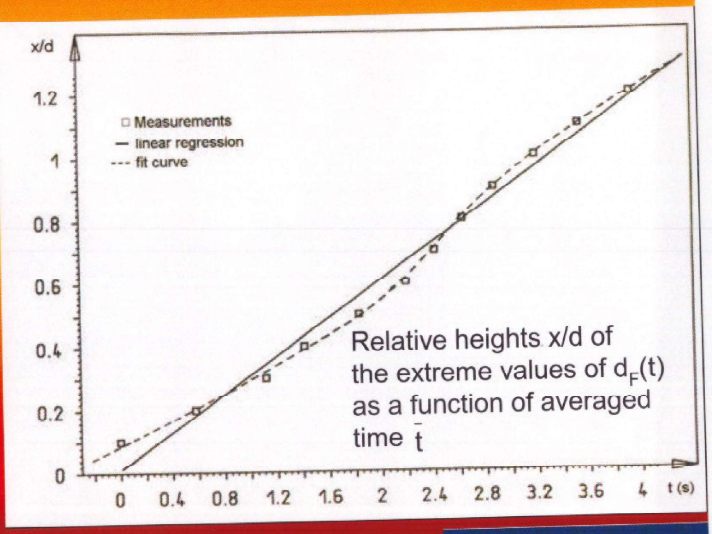


Relative heights x/d of the extreme values of $d_F(t)$ as a function of averaged time $\bar{t}$





## 4.2 Translation velocities of axial parcels

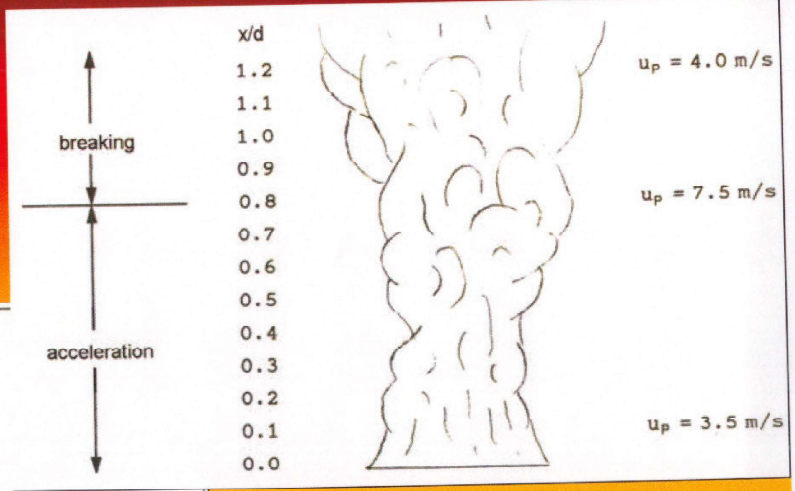


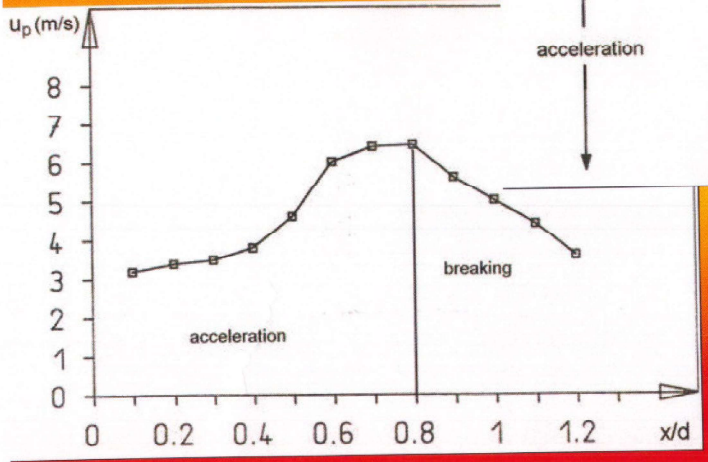


Instantaneous translation velocities $u_p(x/d)$ of rising axial parcels as a function of the relative height x/d; JP-4/gasoline pool fire (d = 16 m)

## 4.2 Translation velocities of axial parcels

| fuel | d (m) | $\bar{u}_p$ (m/s) | standard deviation σ (m/s) |
|---|---|---|---|
| n-pentane | 25 | 8.1 | 1.3 |
| JP-4/gasoline | 25 | 5.5 | 0.4 |
| JP-4/gasoline | 16 | 7.2 | 0.8 |
| JP-4/gasoline | 16 | 4.8 | 0.7 |
| JP-4/gasoline | 8 | 3.6 | 0.4 |
| crude oil | 2.5 | 2.1 | 0.5 |

Averaged transition velocities $\bar{u}_p$ of the rising axial parcels





## 4.3 Rotational velocities of axial parcels

Axial parcels in pool fires show a rotation during their rising movement. The rotation begins in the height range $0.3 < x/d < 0.5$ and reaches a maximum of rotational velocity $\bar{u}_{rot}$ within the acceleration region (Fig. 18). For $0.8 < x/d < 1.0$, the rotational velocity $\bar{u}_{rot}$ decreases.
The rotational velocity depends strongly on meteorological conditions, e.g. wind velocity $u_w$.

| fuel | d (m) | $\bar{\omega}_{rot}$ (rad/s) | $\sigma_{rot}$ (rad/s) | $\bar{u}_{rot}$ (m/s) |
|---|---|---|---|---|
| n-pentane | 25 | 2.4 | 0.44 | 9.6 ($r_{p,max} \approx 4$ m) |
| premium gasoline | 25 | 2.3 | 0.33 | |
| diesel | 25 | 1.8 | 0.32 | |
| JP-4/gasoline | 25 | 1.7 | 0.26 | |
| JP-4/gasoline | 16 | 2.0 | 0.47 | |
| JP-4/gasoline | 8 | 1.9 | 0.33 | |
| diesel | 18 | 2.4 | | 9.6 ($r_{p,max} \approx 4$ m) |

Averaged angular velocities $\bar{\omega}_{rot}$ and averaged rotational velocity $\bar{u}_{rot} = \bar{r}_p \, \bar{\omega}_{rot}$

## 4.3 Rotational velocities of axial parcels

**Determination of the mean radius $\bar{r}_p$ of axial parcels:**

$$r_p = \frac{1}{2}\sqrt{\sigma_F^2} = \frac{1}{2}\sqrt{\Sigma\left(d_F(t) - \bar{d}_F\right)^2 h(d_F)}$$

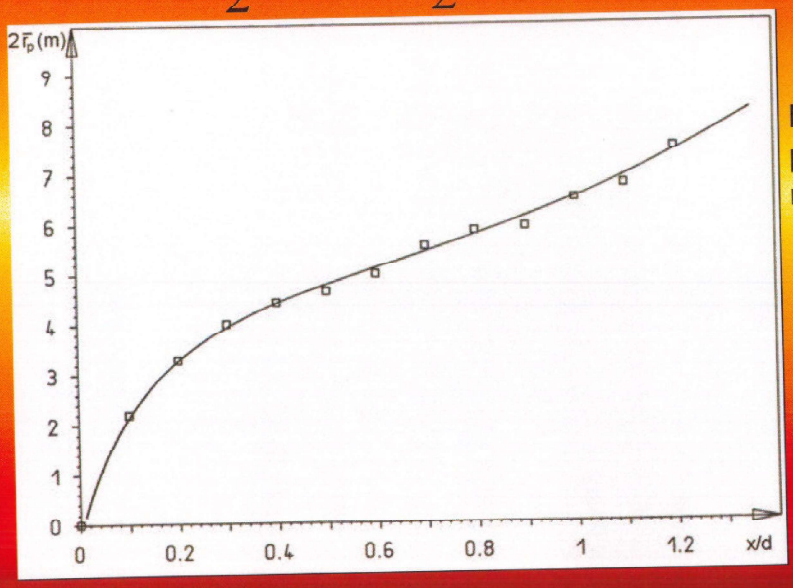


Mean diameter $2\,\bar{r}_p$ of the axial parcels as a function of x/d; n-pentane pool fire (d = 25 m)





## 4.4 Logarithmic probability density function $G_T(T)$ of flame temperatures T

**From a thermographic sequence of IR images for different pool fires a frequency distribution $h_T(T_{I,j})$ of the temperature $T_{i,j}$ of each pixel element is determined.**

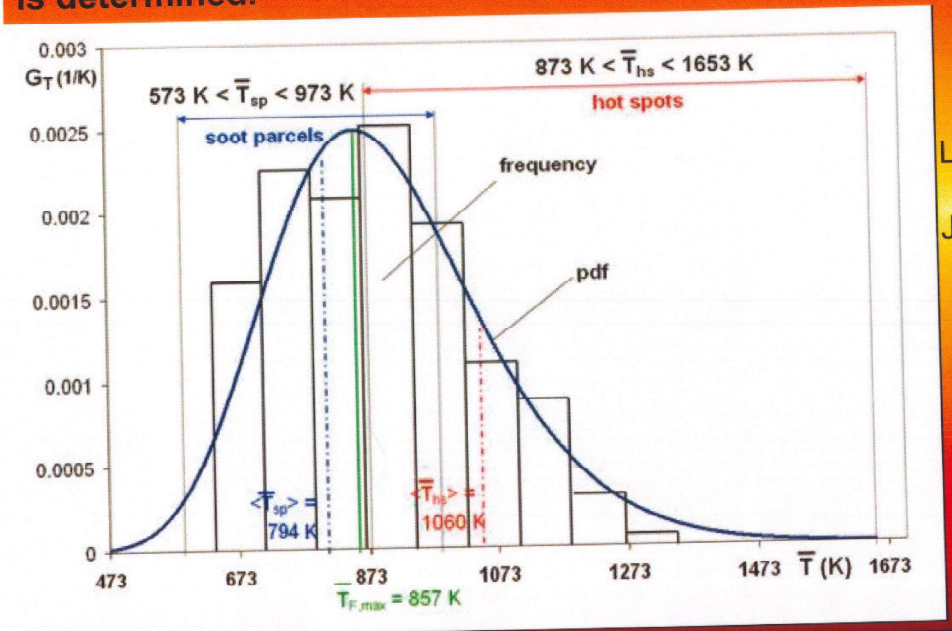


Logarithmic pdf $G_T(\bar{T},d)$

JP-4 pool fire (d = 16 m)

# 4.5 Surface emissive power SEP
## 4.5.1 SEP distribution of a single thermographic image

**Each thermographic image shows an instantaneous temperature distribution and SEP distribution of the fire.**

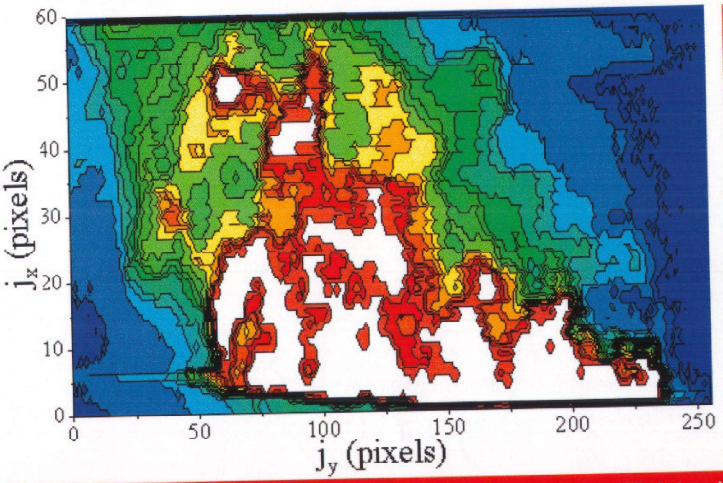


| k | $T_F$ (K) | SEP (kW / m²) |
|---|---|---|
| 15 | (923, 963) | (40.75, 58.37) |
| 14 | (883, 923) | (34.07, 40.75) |
| 13 | (843, 883) | (28.23, 34.07) |
| 12 | (803, 843) | (23.16, 28.23) |
| 11 | (763, 803) | (18.80, 23.16) |
| 10 | (723, 763) | (15.08, 18.80) |
| 9 | (683, 723) | (11.92, 15.08) |
| 8 | (643, 683) | (9.27, 11.92) |
| 7 | (603, 643) | (7.08, 9.27) |
| 6 | (563, 603) | (5.27, 7.08) |
| 5 | (523, 563) | (3.82, 5.27) |
| 4 | (483, 523) | (2.66, 3.82) |
| 3 | (443, 483) | (1.76, 2.66) |
| 2 | (400, 443) | (1.07, 1.76) |
| 1 | (363, 400) | (0.56, 1.07) |
| 0 | (323, 363) | (0.19, 0.56) |

Instantaneous flame surface temperature ($T_F$) isolines and instantaneous surface emissive power (SEP) isolines with k = 0 to k = 15 obtained by a thermographic image, of a JP-4 pool fire (d = 16 m)





## 4.5.2.1 Area fractions of hot spots and soot parcels

$$\bar{a}_{hs}(d) = \int_{\overline{SEP}_1}^{430} G_{SEP}(\overline{SEP})\,d(SEP)$$

$$\bar{a}_{sp}(d) = \int_{6}^{\overline{SEP}_1} G_{SEP}(\overline{SEP})\,d(SEP)$$

with

$\overline{SEP}_1$ = 41.5 kW/m²

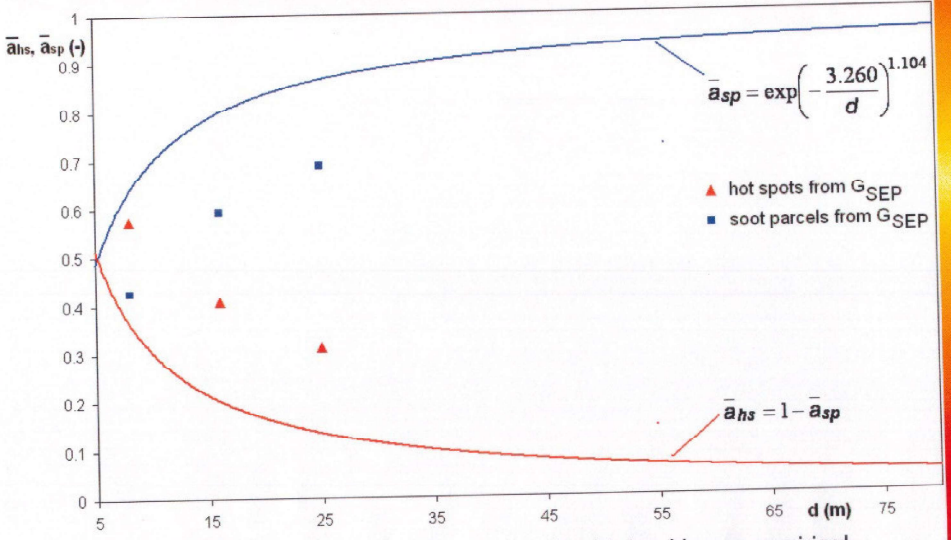


Mean area fractions of hot spots and soot parcels obtained by an empirical correlation and from the pdf $G_{SEP}$(SEP); JP-4 pool fire (d = 16 m)

## 4.5.2 Logarithmic probability density function $G_{SEP}(SEP)$

The temperature $T_{i,j}$ of each pixel element on the thermographic image can be transformed to the surface emissive power $SEP_{i,j}$ by using the relationship:

$$SEP_{i,j}(y,x) = \varepsilon_F \sigma T_{i,j}^4(y,x)$$

The frequency distribution $h_{SEP}(SEP)$ of SEP of the whole flame for different pool fires is determined.

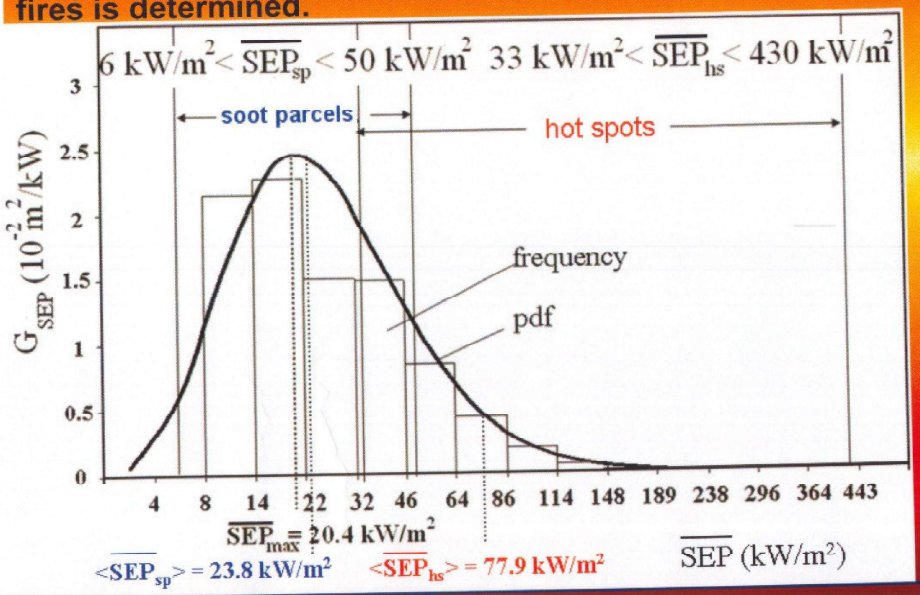


Logarithmic pdf

$G_{SEP}(\overline{SEP}, d)$

JP-4 pool fire (d = 16 m)





## 4.5.3 Irradiance E

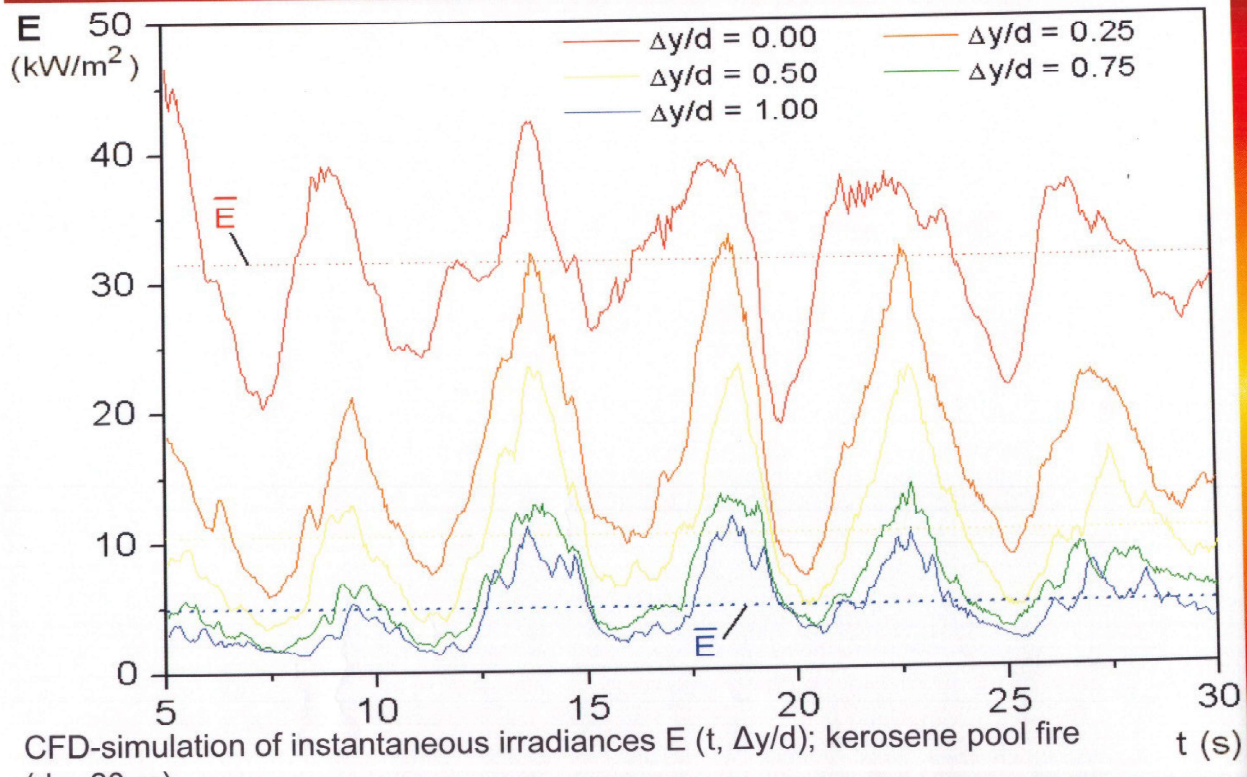


CFD-simulation of instantaneous irradiances E (t, Δy/d); kerosene pool fire (d = 20 m)